# Reliable identification of the auditory thalamus using multi-modal structural analyses

**J. T. Devlin**[1], **E. L. Sillery**[1], **D. A. Hall**[2], **P. Hobden**[1], **T. E. J. Behrens**[1], **R. G. Nunes**[1], **S. Clare**[1], **P. M. Matthews**[1], **D. R. Moore**[2], and **H. Johansen-Berg**[1]

[1] Centre for Functional Magnetic Resonance Imaging of the Brain, University of Oxford, U. K.

[2] MRC Institute of Hearing Research, University Park, Nottingham, U.K.

## Abstract

The medial geniculate body (MGB) of the thalamus is a key component of the auditory system. It is involved in relaying and transforming auditory information to the cortex and in top-down modulation of processing in the midbrain, brainstem, and ear. Functional imaging investigations of this region in humans, however, have been limited by the difficulty of distinguishing MGB from other thalamic nuclei. Here we introduce two methods for reliably delineating MGB anatomically in individuals based on conventional and diffusion MRI data. The first uses high resolution proton-density weighted scanning optimised for subcortical grey-white contrast. The second uses diffusion-weighted imaging and probabilistic tractography to automatically segment the medial and lateral geniculate nuclei from surrounding structures based on their distinctive patterns of connectivity to the rest of the brain. Both methods produce highly replicable results that are consistent with published atlases. Importantly, both methods rely on commonly available imaging sequences and standard hardware, a significant advantage over previously described approaches. In addition to providing useful approaches for identifying the MGB and LGN *in vivo*, our study offers further validation of diffusion tractography for the parcellation of grey matter regions on the basis of their connectivity patterns.

## Keywords

medial geniculate body; lateral geniculate nucleus; proton density; diffusion weighted imaging; tractography

Relative to other sensory systems, a substantial amount of auditory processing occurs subcortically in the brainstem, midbrain, and thalamus (Ehret & Romand, 1997; E. G. Jones, 2003; Winer & Schreiner, 2005). Although the medial geniculate body (MGB) of the thalamus plays a central role in this processing, it has received less attention than other subcortical structures. Nevertheless, a number of animal studies, principally in the cat (reviewed by De Ribaupierre, 1997; Rouiller, 1997), have shown that the mammalian MGB has three major divisions. A ventral division (vMGB) contains large (principal), bi-tufted, thalamocortical 'relay' neurons that typically receive input from the central nucleus of the ipsilateral inferior colliculus and respond transiently, sensitively and discretely to pure tone stimulation of the contralateral ear. Neurons in the medial and dorsal divisions of the MGB typically respond less well to tones than to more complex stimuli and have been implicated in polysensory interactions, processing of communication signals and auditory learning. All three divisions receive descending projections from the cortex that are at least as numerous

Corresponding author: Joseph T. Devlin, Ph. D., FMRIB Centre, Dept. of Clinical Neurology, John Radcliff Hospital, University of Oxford, Headley Way, Headington, Oxford, OX3 9DU, U. K. Phone: +44-(0)1865-222-494 Email: devlin@fmrib.ox.ac.uk.

as the ascending system and that, like other corticothalamic projections, have been implicated in gain control, signal filtering and other dynamic functions. As understanding of the importance of top-down processing in the brain expands, the MGB is receiving increasing attention because of its position at the cross-roads of auditory processing (Winer, Miller, Lee, & Schreiner, 2005).

These animal studies typically rely on invasive techniques precluding their use in humans except in intra-operative studies (cf. Celesia, 1976; Yvert et al., 2002). Although functional magnetic resonance imaging (fMRI) offers the potential to study these processes non-invasively, a number of technical challenges limit its efficacy. These include the acoustic noise of the scanner (often >90dB SPL), pulsatile motion effects in subcortical structures, and significant spatial resolution difficulties identifying specific thalamic nuclei. Sparse, or clustered, acquisition techniques offer a solution to the problem of scanner noise (Eden, Joseph, Brown, Brown, & Zeffiro, 1999; Edmister, Talavage, Ledden, & Weisskoff, 1999; Hall et al., 1999) while cardiac gated acquisition helps to reduce the variability associated with pulsatile motion (Guimaraes et al., 1998). There are, however, no established methods for reliably identifying some anatomical regions of the ascending auditory system, including the MGB. Studies to date have relied on using functional imaging results to localize nuclei in individual subjects, which risks defining the regions on the basis of the properties being explored (Giraud et al., 2000). Alternately, it can be assumed that individual variations are modest and published atlases used (Griffiths, Uppenkamp, Johnsrude, Josephs, & Patterson, 2001; Harms & Melcher, 2002). In principle, however, this obscures inter-subject anatomic variability (Morel, Magnin, & Jeanmonod, 1997; Niemann, Mennicken, Jeanmonod, & Morel, 2000; Rademacher, Burgel, & Zilles, 2002), which could reduce sensitivity, and even lead to inaccurate localisations. Consequently, a reliable anatomical method for identifying MGB in individuals is an important step towards better functional characterisation of this region in humans.

Despite excellent anatomic resolution of typical T1 or T2 weighted human structural MRI scans, the individual nuclei of the thalamus are not distinct in these images, making it difficult to identify MGB from adjacent structures. Magnotta et al. (2000) reported that using an inversion recovery sequence that selectively nulls signal from grey matter allows for visualisation of distinct nuclei within the thalamus. Although the geniculate bodies were visible using this sequence, the boundary between them was not apparent. More recently, Deoni and colleagues (2005) have shown that is possible to identify individual thalamic nuclei based on a combination of their T1 and T2 signatures using very high resolution structural images ($700\mu m^3$ isotropic voxels), but this required approximately 13 hours of scanning for a single subject at 1.5T. Much higher field strengths (4–8 tesla) improve the contrast between nuclei and reduce scanning time, but these scanners are not commonly available (Bourekas et al., 1999; Deoni, Josseau et al., 2005).

Here, we test two alternative approaches to identifying MGB anatomically based on commonly available pulse sequences on standard hardware. The first uses proton-density (PD) weighted images to enhance grey-white contrast in the thalamus. Because proton density in grey matter is approximately 20% greater than in white matter (Wood, Bronskill, Mulkern, & Santyr, 1994) one can better distinguish the border between the medial and lateral geniculate nuclei (Fujita et al., 2001). The second approach uses diffusion-weighted imaging (DWI) and tractography to differentiate the MGB and LGN. These two nuclei relay auditory and visual information to primary auditory and visual cortices, respectively, and consequently have distinct patterns of connectivity. Thus it should be possible to distinguish the two based solely on their anatomical connectivity profiles (Behrens, Johansen-Berg et al., 2003). Here we evaluate these two anatomical methods for identifying MGB in individuals for both consistency and reliability.

## Materials and methods

Five neurologically normal volunteers (3F, 2M) participated in two separate scanning sessions each lasting approximately one hour. Although no task was performed in either session, we verified that all participants had normal hearing (pure tone average 20 dB HL) to rule out any structural changes associated with hearing loss. Each gave informed consent after the experimental methodology was explained and the experiments were approved by the Central Oxford Research Ethics Committee.

Proton density scans were acquired on a Siemens Sonata 1.5T scanner at the Oxford Centre for Clinical Magnetic Resonance Research (OCMR). Slices were acquired coronally with a $800\mu m \times 800\mu m$ in-plane resolution and a slice thickness of 2mm using a fast spin echo protocol (TR = 6s, effective TE = 9.5msec). The use of a long repetition time and a short echo time minimized the T1 and T2 weighting, leaving proton density as the primary source of tissue contrast (Jackson, Ginsberg, Schomer, & Leeds, 1997). For each participant, between 5 to 8 scans were acquired, realigned and averaged to increase the signal-to-noise ratio (SNR) associated with smaller voxel sizes. Each PD scan took approximately 9 minutes. In addition, a standard T1-weighted structural scan (3D Turbo FLASH, TR=12ms, TE=5.6ms, $1mm^3$ isotropic voxels) was also acquired.

Diffusion weighted scans were acquired on a Varian-Siemens 3T scanner with a maximum gradient strength of $22mT \cdot m^{-1}$ at the Functional Magnetic Resonance Imaging of the Brain (FMRIB) Centre in Oxford. The protocol used a doubly-refocused spin-echo sequence to minimise eddy currents (Reese, Heid, Weisskoff, & Wedeen, 2003) and cardiac gating to minimize pulsatile motion artefacts (Nunes, Jezzard, & Clare, 2005). Each data set consisted of 3 non-diffusion-weighted and 60 diffusion-weighted images acquired with a *b* value of $1000 \text{ s} \cdot mm^{-2}$. The diffusion gradients were uniformly distributed through space using a scheme optimised for white matter (D. K. Jones, Horsfield, & Simmons, 1999) and the echo time was set to 106 msec with an effective repetition time of 20 R-R intervals. Each set of images contained 60 contiguous slices with a 2.5 mm thickness. A half k-space acquisition was performed with a matrix size set to $62 \times 96$ and a field of view of $240 \times 240 \text{ mm}^2$. The images were interpolated to achieve a matrix size of $128 \times 128$ and a final resolution of $1.875 \times 1.875 \times 2.5 \text{ mm}^3$. The acquisition time depended on heart rate but was approximately 20mins per scan. Three complete data sets were acquired per participant and were corrected for eddy currents and head motion using an affine registration to the reference image (Jenkinson & Smith, 2001). Data from the three acquisitions were averaged to improve the SNR and then probability distributions based on the fibre orientations were calculated at each voxel using FDT (www.fmrib.ox.ac.uk/fsl) (Behrens, Woolrich et al., 2003).

### Identification of MGB based on proton-density MR contrast

In the PD, but not the T1 scan, both the lateral and medial geniculate nuclei were visible in coronal sections. Based on relations to landmark structures in a standard anatomical atlas (Duvernoy, 1995), the MGB could be identified on individual scans and borders with LGN defined. Figure 1 presents the two illustrative coronal sections used in visual identification with the relevant anatomical landmarks labelled. The left-most panels are photographs of unstained, post-mortem tissue cut perpendicular to the AC-PC plane (modified from Duvernoy, 1995 pp. 292, 301). The middle panels are PD-weighted images through identical planes (but from a different brain) showing many of the same structures present in the tissue section. The right-most panels are the corresponding T1 images from the same subject. Note that the relative contrast is lower, making it difficult to identify individual structures with confidence, despite excellent contrast for cerebral grey-white borders (not shown). Some of

the improvement in the resolving power in the PD image came from increased in-plane resolution, but the greatest effects were due to enhanced grey-white contrast in these areas.

Using these sections, MGB was identified independently by three of the authors (JTD, DAH, HJB) in the native space of each participant's PD scan using the following procedure. We began by first finding the coronal slice showing the substantia nigra (SN) meeting at the interpeduncular fossa (approximately Y= −22 when transformed into standard space, Figure 1, top row). The SN appears as a region of high intensity running infero-medially from the thalamus (Th), inferior to the third ventricle (V3). In each subject, Heschl's gyrus was visible bilaterally in this slice (not shown). We then moved 6–10mm caudally until the LGN appeared as a tear-dropped shape region of high intensity superior and medial to the body of the hippocampus (Hi) and inferolateral to the majority of the thalamus. The MGB was immediately medial to the LGN and appeared as an oval region of high intensity. The border with LGN was easily visible and appeared in the PD images as a thin dark strip separating the two high intensity regions (Figures 1 & 3) and corresponds to a thin band of myelinated fibres (Hassler, 1982). The dorso-medial border was less clear, and consequently we relied on the fact that MGB is roughly ovoid to complete the border. It is worth noting that even in post-mortem tissue stained for either cell bodies (Nissl) or for acetylcholinesterase (AChE) these borders are indistinct (Hirai & Jones, 1989). There is a gradual transition from MGB to the suprageniculate nucleus medially and from MGB to the posterior nucleus dorso-medially (Hirai & Jones, 1989), following the nomenclature of Jones (1985).

Masks were drawn in each hemisphere to separately cover MGB and LGN, which were typically visible on between one and three slices.

### Identification of MGB based on connectivity patterns from diffusion tractography

Given the difficulty in identifying a precise dorso-medial border for MGB in either the PD images or in stained tissue, an alternate possibility is to delineate MGB and LGN based on their distinct patterns of connectivity. As mentioned previously, MGB receives inputs from the central nucleus of the ipsilateral inferior colliculus and has reciprocal connections with primary auditory cortex via the acoustic radiation. In contrast, LGN receives afferent projections from retinal ganglion cells via the optic tract and has bi-directional connections with primary visual cortex via the optic radiation. Consequently, it should be possible to separate the two geniculate nuclei based solely on their distinct patterns of connectivity. Recently, Johansen-Berg and colleagues (2004) demonstrated that it is possible to identify a functionally meaningful border between the supplemental motor area (SMA) and pre-SMA, based solely on their respective connectivity profiles using probabilistic tractography. In other words, anatomical pathways were identified from a set of voxels that included both SMA and pre-SMA regions, and based solely on the pattern of connections, the voxels were segmented into two distinct clusters. Importantly, this connectivity-based segmentation corresponded closely to a delineation of the regions based on their different functional response properties. We tested whether the same approach could be applied to separating the medial and lateral geniculate.

We began by defining a region-of-interest (ROI) in the standard space defined by the Montreal Neurological Institute 152-mean brain. The coordinates were X= ±10 to 26 medial-laterally, Y= −22 to −30 rostro-caudally, and Z= −2 to −10 superior-inferiorly. This region was chosen to conservatively include both MGB and LGN based on previously published coordinates (Griffiths et al., 2001; Niemann et al., 2000; Rademacher et al., 2002). When previous studies used a version of the Talaraich and Tournoux (1988) stereotaxic reference system rather than the MNI system, these coordinates were transformed into MNI-space (Brett, Johnsrude, & Owen, 2002).

Probabilistic tractography (Behrens, Woolrich et al., 2003) was run from each voxel in the mask and tracts were limited to the ipsilateral hemisphere. Voxels within the hemisphere were classified as connected to the seed voxel if the probability of connection was greater than 0.1%. Additional analyses with different thresholds (1%, 10%) did not alter the basic findings. These connections were stored in a M × N connectivity matrix, where M was the number of seed voxels and N was the number of voxels in the hemisphere. Each cell of the connectivity matrix ([$i$, $j$]) was set to 1 if tractography revealed an anatomical path linking seed voxel $i$ to hemisphere voxel $j$, and set to 0 otherwise. To reduce the storage requirements, this space was down-sampled from isotropic 2mm to isotropic 3mm resolution, but only for storing the results. A symmetric M × M cross-correlation matrix was then computed as a measure of voxel-wise similarity of connectivity patterns of seed voxels. That is, the value in cell [$i$, $j$] in the cross-correlation matrix represented the correlation in connectivity between voxels $i$ and $j$ of the original seed mask.

At this stage, the matrix has no meaningful structure because cells were arbitrarily ordered. Structure was introduced into the matrix by permuting the nodes using a spectral reordering algorithm (Barnard, Pothen, & Simon, 1995; Johansen-Berg et al., 2004) which forces large values (i.e. high correlations) to the diagonal. As a consequence, voxels with similar connectivity cluster together and can be identified directly in the sorted cross-correlation matrix. These clusters were identified by eye as groups of elements that are strongly correlated with each other and weakly correlated with the rest of the matrix. Elements that did not clearly belong to a single cluster were left unclassified. The cells in each cluster were then mapped back onto their original anatomical locations in each individual's T1 weighted structural image, after registration into standard space (Jenkinson & Smith, 2001). The procedure is schematized in Figure 2. If the clusters from the re-ordered cross correlation matrix correspond to anatomical clusters in the T1 image, then this provides evidence that the particular anatomical region has a relatively homogenous pattern of connectivity that differs from that of other clusters. Thus, despite non-geniculate voxels in the seed mask, the two strongest clusters are expected to correspond to the medial and lateral geniculate, as these two regions are the only complete thalamic nuclei in the mask. It is worth noting that this method does not necessarily require complete tracing of pathways to their final destinations – only that the connectivity patterns from MGB and LGN are distinct (Johansen-Berg et al, 2004).

## Results

### Identification based on proton-density MR contrast

In all ten hemispheres, MGB was identified visually (Figure 3). To determine the consistency and reliability of these manually drawn masks, the centre of gravity was computed for each mask. The average distance between the corresponding centre of gravity across the three raters was 1.3mm and varied from 0.3 to 2.4mm. In other words, the grey-white contrast in the high resolution PD scans coupled with a clear procedure for identifying MGB led to a consistent mask, independent of the person doing the identification. In standard space coordinates, the mean (±SEM) centre of gravity for MGB were [X= −15 (1.2), Y= −28 (1.7), Z= −8 (1.4)] in the left hemisphere and [X= +16 (1.2), Y= −27 (1.5), Z= −7 (1.2)] in the right hemisphere (Table). These values correspond closely to published coordinates for MGB (Morel et al., 1997; Niemann et al., 2000; Rademacher et al., 2002).

The same procedures were used to evaluate consistency in the LGN masks. The average distance between corresponding centres of gravity across the raters was 1.4mm and varied from 0.2 to 2.9mm. In standard space coordinates, the mean (±SEM) centre of gravity for LGN were [X= −21 (1.6), Y= −27 (1.8), Z= −8 (1.1)] in the left hemisphere and [X= +23

(1.5), Y= −27 (2.0), Z= −7 (1.0)] in the right hemisphere, congruent with the thalamic atlas of Morel (1997).

In order to determine the minimal amount of data necessary to maintain these results, the same method was applied to averaged PD-scans based on either 2, 3, 4, or 5 images per subject (i.e. between 10–50 mins. of data acquisition). Masks were then drawn independently by two of the authors (JTD, HJB) who were blind to the number of scans used to generate each image. Surprisingly, the centres-of-gravity did not significantly change across the 2–5 scan averages – the variability was comparable to that seen between raters (1–2mm). Anecdotally, however, raters reported poor confidence in their masks for images based on only two scans. In other words, three scans appeared to be minimum number of PD scans necessary per participant in order to visually identify MGB and LGN with confidence.

## Identification based on changes in connectivity patterns from diffusion tractography

In all subjects, re-ordered cross correlation matrices contained clearly identifiable clusters for each hemisphere (Figure 4). When these were projected back onto the brain, the two strongest clusters (i.e. those at either end of the diagonal) corresponded to medial and lateral divisions of the original ROI. The fact that the clusters were in opposite corners of the re-ordered cross-correlation matrix indicates that in each case, the two regions had the most dissimilar patterns of connectivity. The coordinates of the centres of these clusters were consistent with those found in the PD image localisations: the mean centre of gravity for the medial clusters was [X= −14 (0.4), Y= −25 (0.4), Z= −6 (0.2)] in the left hemisphere and [X= +13 (0.2), Y= −25 (0.6), Z= −7 (0.2)] in the right hemisphere, and correspond closely to published coordinates for MGB (Morel et al., 1997; Niemann et al., 2000; Rademacher et al., 2002). Similarly, the mean centre of gravity coordinates for the lateral cluster were [X= −22 (1.1), Y= −27 (0.4), Z= −6 (0.3)] in the left hemisphere and [X= +21 (0.8), Y= −27 (0.6), Z= −6 (0.6)] in the right hemisphere, consistent with the location of LGN (Fujita et al., 2001).

In order to further test whether these clusters correspond to MGB and LGN, respectively, connectivity from each region was evaluated using probabilistic tractography. The connectivity profile of each cluster was mapped by seeding the centre of gravity and recording the resulting anatomical paths (Figure 5). There was consistently a clear subcortical path linking the medial region to the ipsilateral inferior colliculus (IC), which continued on to both the contralateral and ipsilateral cochlear nucleus (CN). This pattern is consistent with predominantly contralateral connections from CN to IC and the weaker, but well studied, ipsilateral IC to CN projections. (Moore, 1991). The tectothalamic projections from IC, on the other hand, are purely ipsilateral (Winer, Chernock, Larue, & Cheung, 2002), exactly as seen in the tractography results. We did not, however, identify the acoustic radiation linking MGB to Heschl's gyrus, the site of primary auditory cortex. The single fibre diffusion model used here (Behrens, Woolrich et al., 2003) is sensitive primarily to major pathways and therefore smaller pathways, or paths that cross other tracts, are not always detected. The acoustic radiation penetrates the much larger internal capsule (Rademacher et al., 2002) and so the fact that we do not find it here is not unexpected. Use of more complex fibre models (Parker & Alexander, 2003; Tuch, Reese, Wiegell, & Wedeen, 2003) may increase sensitivity to such pathways. In contrast, thalamocortical projections through Meyer's loop were clearly present linking the lateral cluster to posterior occipital regions, consistent with the LGN's role as a visual relay station (cf. Ciccarelli et al., 2003). In other words, the pattern of connectivity observed for the medial and lateral clusters strongly suggests that these regions correspond to MGB and LGN, respectively.

Finally, to determine the minimum data required to identify the geniculate bodies, the DTI-based segmentation was re-run using only a single DTI run (i.e. 20 min of data) per

participant. Because segmentation relies on different patterns of connectivity, rather than on completely specifying individual tracts, we anticipated the method would be robust to the lower SNR in the single data set and this was born out by the results. In all cases, there were clear clusters in the reordered cross correlation matrices corresponding to the medial and lateral geniculate bodies. Moreover, the centre-of-gravity of these clusters did not significantly differ from those in the original analyses in any direction (all $t_{19} < 1.0$, n.s.). In other words, a single 20 min. data acquisition was sufficient to reliably identify MGB from LGN using this technique. We were, however, unable to reliably trace paths from the centre of these clusters, as the lower SNR translated into greater uncertainty in the probabilistic tractography algorithm.

### Consistency between methods

Finally, the DWI-based MGB and LGN clusters were compared to those derived from the PD images to determine the consistency between methods. In Figure 6, the standard space coordinates of the centre of gravity (COG) for each nucleus per subject were plotted in the X and Z planes for both segmentation methods. 85% confidence intervals are shown as large ovals surrounding each cluster. In the left hemisphere, COGs based on PD-segmentations were on average 1.5mm more inferior than DTI-based values but did not differ on the medial-to-lateral axis. In the right hemisphere, PD-based values were, on average, 2.1mm more lateral than DTI-based values. They did not, however, differ in the inferior-to-superior axis. In both cases, the displacement was approximately the size of one DTI voxel (2mm). It is possible that these differences were driven, in part, by a systematic bias when drawing the MGB masks on the PD images towards the more clearly visible lateral and inferior regions, although differences in the registration process could also account for some of this variance. The results presented here are similar to those reported by Johansen-Berg and colleagues (2004) who found that connectivity-based segmentations of SMA and pre-SMA were approximately 2mm different from segmentations based on activation of the regions using fMRI.

## Discussion

We have demonstrated two methods for reliably identifying MGB based solely on structural MR data. The first relies on differences in proton density between grey and white matter while the second is based on the distinct connectivity profiles of the medial and lateral geniculate. Identifying MGB based on PD images required a minimum of 30 minutes of data acquisition in order to be confident in the visual identification process. Additional data (up to 50mins.) helped improve the clarity of the borders but further data acquisition (60+ mins.) led to diminishing returns. Morphometric studies would no doubt benefit from the extra signal-to-noise ratio (SNR) in the 50min data whereas simple localisation of MGB for fMRI can be accomplished with only 30mins. of data acquisition. The DTI-based segmentation was robust with only a single, 20min run of data but adequate tractography required better SNR which was obtained by averaging three 20min. runs. It is worth noting, however, that the DTI data were acquired on a fairly old 3T scanner (circa 1997) with limited SNR. Pilot testing with data from a current generation Siemens Allegra 1.5T scanner showed that two 9-minute runs of DWI data had a 25% *increase* in SNR relative to our original three runs of 20 min each. In other words, with a modern scanner it should be possible to acquire sufficient DTI data in 9mins to adequately segment MGB from LGN. Furthermore, in both cases, data acquisition used commonly available pulse sequences on standard hardware. Thus, there was a clear advantage over approaches that rely on either extremely long acquisitions (Deoni, Josseau et al., 2005) or very high fields (Bourekas et al., 1999; Deoni, Josseau et al., 2005).

The current study builds on previous anatomical analyses of thalamus which have used diffusion weighted imaging. Wiegell and colleagues (2003), for instance, used local fibre orientation to identify major thalamic nuclei while Behrens and colleagues (2003) used thalamocortical projection zones. In both cases, although the larger nuclei were easily identified, it was difficult to reliably distinguish between MGB and LGN. In contrast, by focusing our analyses specifically on these two nuclei, including subcortical pathways, and using a method that does not require complete tracing of pathways to their final destinations, we were able to show clear distinctions between the two. The fact that our DWI-derived masks of MGB closely matched the manually identified regions provides further validation of this connectivity-based segmentation approach (Johansen-Berg et al., 2004).

It is also worth considering the limitations of the current study and how these might be addressed in the future. First, the medial and dorso-medial borders of MGB were not clearly delineated in the PD images and consequently this portion of the MGB masks was somewhat arbitrary. Indeed, this may contribute to the small differences observed between the PD and DTI identifications of the MGB. Recent advances in steady state imaging techniques (Deoni, Peters, & Rutt, 2005), however, offer the potential for supplementing high resolution PD images with simultaneously acquired T1 and T2 maps, thus combining the strengths of Deoni and colleagues' (2005) multi-spectral approach with the current anatomical identifications of MGB and LGN, all within a single 1-hour scanning session. *In vivo* morphometric analyses of MGB would certainly benefit from this additional anatomical clarity. Second, the accuracy of the borders identified using our connectivity-based segmentation scheme was limited by the resolution of the DTI images (roughly $10\text{mm}^3$) which is fairly coarse given the size and shapes of the medial and lateral geniculate nuclei (approximately 90 and $115\text{mm}^3$, respectively, Morel et al., 1997; Winer, 1984 and current findings) introducing significant partial volume effects. Smaller voxel sizes, however, significantly reduce the signal-to-noise ratio in DWI data, thus increasing uncertainty and reducing the likelihood of tracing a path to its final destination. A major strength of the connectivity-based parcellation technique used here, however, is that it does not require complete paths – only that the pattern of connectivity differs across regions. Consequently, the method should be equally robust at delineating the two regions despite reduced SNR and the increased spatial resolution should improve accuracy at the borders of the regions.

The ability to reliably identify MGB in individuals provides improved anatomical localisation for functional investigations of the auditory thalamus. Many studies have already shown that fMRI can be successfully used to detect MGB activation to both simple and complex auditory stimuli (Budd et al., 2003; Guimaraes et al., 1998; Krumbholz et al., 2005; Lockwood et al., 1999; Maeder et al., 2001), but comparative investigations of MGB's specific contributions to auditory processing in humans are less common (but see Giraud et al., 2000; Griffiths et al., 2001; Harms & Melcher, 2002). For instance, we have demonstrated a surprising left cortical dominance for monaural processing of simple tones, and preliminary analyses suggest this may arise at the level of the MGB (Devlin et al., 2003; Moore et al., 2004). The inability to reliably identify MGB anatomically, however, limited the sensitivity of our analyses and may bias the results. The anatomical methods present here combined with higher resolution functional imaging more suited to imaging such a small structure (Beauchamp, Argall, Bodurka, Duyn, & Martin, 2004; Bridge et al., 2005), will hopefully complement, extend, and objectify further functional characterisations of this increasingly interesting nuclear group.

## Acknowledgments

# References

Barnard ST, Pothen A, Simon HD. Numer Linear Algebra Appl. 1995; 2:317–334.

Beauchamp MS, Argall BD, Bodurka J, Duyn JH, Martin A. Unraveling multisensory integration: patchy organization within human STS multisensory cortex. Nat Neurosci. 2004; 7(11):1190–1192. [PubMed: 15475952]

Behrens TEJ, Johansen-Berg H, Woolrich MW, Smith SM, Wheeler-Kingshott CA, Boulby PA, et al. Non-invasive mapping of connections between human thalamus and cortex using diffusion imaging. Nat Neurosci. 2003; 6(7):750–757. [PubMed: 12808459]

Behrens TEJ, Woolrich MW, Jenkinson M, Johansen-Berg H, Nunes RG, Clare S, et al. Characterization and propagation of uncertainty in diffusion-weighted MR imaging. Magn Reson Med. 2003; 50(5):1077–1088. [PubMed: 14587019]

Bourekas EC, Christoforidis GA, Abduljalil AM, Kangarlu A, Chakeres DW, Spigos DG, et al. High resolution MRI of the deep gray nuclei at 8 Tesla. J Comput Assist Tomogr. 1999; 23(6):867–874. [PubMed: 10589560]

Brett M, Johnsrude IS, Owen AM. The problem of functional localization in the human brain. Nat Rev Neurosci. 2002; 3(3):243–249. [PubMed: 11994756]

Bridge H, Clare S, Jenkinson M, Jezzard P, Parker AJ, Matthews PM. Independent anatomical and functional measures of the V1/V2 boundary in human visual cortex. J Vis. 2005; 5(2):93–102. [PubMed: 15831070]

Budd TW, Hall DA, Goncalves MS, Akeroyd MA, Foster JR, Palmer AR, et al. Binaural specialisation in human auditory cortex: an fMRI investigation of interaural correlation sensitivity. Neuroimage. 2003; 20(3):1783–1794. [PubMed: 14642488]

Celesia GG. Organization of auditory cortical areas in man. Brain. 1976; 99:403–414. [PubMed: 1000279]

Ciccarelli O, Toosy AT, Parker GJ, Wheeler-Kingshott CA, Barker GJ, Miller DH, et al. Diffusion tractography based group mapping of major white-matter pathways in the human brain. Neuroimage. 2003; 19(4):1545–1555. [PubMed: 12948710]

De Ribaupierre, F. (1997). Acoustical information processing in the auditory thalamus and cerebral cortex. In G. Ehret & R. Romand (Eds.), *The Central Auditory System* (pp. 317–397). New York: Oxford University Press.

Deoni, S. C., Josseau, M. J., Rutt, B. K., & Peters, T. M. (2005). Visualization of thalamic nuclei on high resolution, multi-averaged T(1) and T(2) maps acquired at 1.5 T. *Hum Brain Mapp*

Deoni SC, Peters TM, Rutt BK. High-resolution T1 and T2 mapping of the brain in a clinically acceptable time with DESPOT1 and DESPOT2. Magn Reson Med. 2005; 53(1):237–241. [PubMed: 15690526]

Devlin JT, Raley J, Tunbridge E, Lanary K, Floyer-Lea A, Narain C, et al. Functional asymmetry for auditory processing in human primary auditory cortex. J Neurosci. 2003; 23(37):11516–11522. [PubMed: 14684855]

Duvernoy, H. (1995). *Human Brain Stem and Cerebellum: Surface, Structure, Vascularization, and Three-Dimensional Sectional Anatomy With MRI* New York: Springer-Verlag.

Eden GF, Joseph JE, Brown HE, Brown CP, Zeffiro TA. Utilizing hemodynamic delay and dispersion to detect fMRI signal change without auditory interference: The behavior interleaved gradients technique. Magnetic Resonance in Medicine. 1999; 41:13–20. [PubMed: 10025606]

Edmister WB, Talavage TM, Ledden PJ, Weisskoff RM. Improved auditory cortex imaging using clustered volume acquisitions. Hum Brain Mapp. 1999; 7(2):89–97. [PubMed: 9950066]

Ehret, G., & Romand, R. (Eds.). (1997). *The Central Auditory System* New York: Oxford University Press.

Fujita N, Tanaka H, Takanashi M, Hirabuki N, Abe K, Yoshimura H, et al. Lateral geniculate nucleus: anatomic and functional identification by use of MR imaging. AJNR Am J Neuroradiol. 2001; 22(9):1719–1726. [PubMed: 11673167]

Giraud AL, Lorenz C, Ashburner J, Wable J, Johnsrude I, Frackowiak R, et al. Representation of the temporal envelope of sounds in the human brain. Journal of Neurophysiology. 2000; 84:1588–1598. [PubMed: 10980029]

Griffiths TD, Uppenkamp S, Johnsrude I, Josephs O, Patterson RD. Encoding of the temporal regularity of sound in the human brainstem. Nat Neurosci. 2001; 4(6):633–637. [PubMed: 11369945]

Guimaraes AR, Melcher JR, Talavage TM, Baker JR, Ledden P, Rosen BR, et al. Imaging subcortical auditory activity in humans. Human Brain Mapping. 1998; 6:33–41. [PubMed: 9673661]

Hall DA, Haggard MP, Akeroyd MA, Palmer AR, Summerfield AQ, Elliot MR, et al. "Sparse" temporal sampling in auditory fMRI". Human Brain Mapping. 1999; 7:213–223. [PubMed: 10194620]

Harms MP, Melcher JR. Sound repetition rate in the human auditory pathway: representations in the waveshape and amplitude of fMRI activation. J Neurophysiol. 2002; 88(3):1433–1450. [PubMed: 12205164]

Hassler, R. (1982). Architectonic organisation of the thalamic nuclei. In G. Schaltenbrand & A. E. Walker (Eds.), *Stereotaxy of the Human Brain* (pp. 140–180). New York: Thieme.

Hirai T, Jones EG. A new parcellation of the human thalamus on the basis of histochemical staining. Brain Res Brain Res Rev. 1989; 14(1):1–34. [PubMed: 2720229]

Jackson EF, Ginsberg LE, Schomer DF, Leeds NE. A review of MRI pulse sequences and techniuqes used in neuroimaging. Surgical Neurology. 1997; 47:185–199. [PubMed: 9040824]

Jenkinson M, Smith SM. A global optimisation method for robust affine registration of brain images. Medical Image Analysis. 2001; 5(2):143–156. [PubMed: 11516708]

Johansen-Berg, H., Behrens, T. E., Robson, M. D., Drobnjak, I., Rushworth, M. F., Brady, J. M., et al. (2004). Changes in connectivity profiles define functionally distinct regions in human medial frontal cortex. *Proc Natl Acad Sci U S A*

Jones DK, Horsfield MA, Simmons A. Optimal strategies for measuring diffusion in anisotropic systems by magnetic resonance imaging. Magn Reson Med. 1999; 42(3):515–525. [PubMed: 10467296]

Jones, E. G. (1985). *The Thalamus* New York: Plenum Press.

Jones EG. Chemically defined parallel pathways in the monkey auditory system. Ann N Y Acad Sci. 2003; 999:218–233. [PubMed: 14681146]

Krumbholz K, Schonwiesner M, Rubsamen R, Zilles K, Fink GR, von Cramon DY. Hierarchical processing of sound location and motion in the human brainstem and planum temporale. Eur J Neurosci. 2005; 21(1):230–238. [PubMed: 15654860]

Lockwood AH, Salvi RJ, Coad ML, Arnold SA, Wack DS, Murphy BW, et al. The functional anatomy of the normal human auditory system: responses to 0.5 and 4.0 kHz tones at varied intensities. Cereb Cortex. 1999; 9(1):65–76. [PubMed: 10022496]

Maeder PP, Meuli RA, Adriani M, Bellmann A, Fornari E, Thiran JP, et al. Distinct pathways involved in sound recognition and localization: a human fMRI study. Neuroimage. 2001; 14(4):802–816. [PubMed: 11554799]

Magnotta VA, Gold S, Andreasen NC, Ehrhardt JC, Yuh WT. Visualization of subthalamic nuclei with cortex attenuated inversion recovery MR imaging. Neuroimage. 2000; 11(4):341–346. [PubMed: 10725190]

Moore DR. Anatomy and physiology of binaural hearing. Audiology. 1991; 30(3):125–134. [PubMed: 1953442]

Moore, D. R., Devlin, J. T., Raley, J., Tunbridge, E., Lanary, K., Floyer-Lea, A., et al. (2004). Effects of long term unilateral hearing loss on the lateralization of fMRI measured activation in human auditory cortex. In J. Syka & M. M. Merzenich (Eds.), *Plasticity of the Central Auditory System and Processing of Complex Acoustic Signals*: Klewer Plenum.

Morel A, Magnin M, Jeanmonod D. Multiarchitectonic and stereotactic atlas of the human thalamus. J Comp Neurol. 1997; 387(4):588–630. [PubMed: 9373015]

Niemann K, Mennicken VR, Jeanmonod D, Morel A. The Morel stereotactic atlas of the human thalamus: atlas-to-MR registration of internally consistent canonical model. Neuroimage. 2000; 12(6):601–616. [PubMed: 11112393]

Nunes RG, Jezzard P, Clare S. Investigations on the efficiency of cardiac-gated methods for the acquisition of diffusion-weighted images. J Magn Reson. 2005; 177(1):102–110. [PubMed: 16112886]

Parker GJ, Alexander DC. Probabilistic Monte Carlo based mapping of cerebral connections utilising whole-brain crossing fibre information. Inf Process Med Imaging. 2003; 18:684–695. [PubMed: 15344498]

Rademacher J, Burgel U, Zilles K. Stereotaxic localization, intersubject variability, and interhemispheric differences of the human auditory thalamocortical system. Neuroimage. 2002; 17(1):142–160. [PubMed: 12482073]

Reese TG, Heid O, Weisskoff RM, Wedeen VJ. Reduction of eddy-current-induced distortion in diffusion MRI using a twice-refocused spin echo. Magn Reson Med. 2003; 49(1):177–182. [PubMed: 12509835]

Rouiller, E. M. (1997). Functional organization of the auditory pathways. In G. Ehret & R. Romand (Eds.), *The Central Auditory System* (pp. 3–96). New York: Oxford University Press.

Talairach, J., & Tournoux, P. (1988). *Co-planar stereotaxic atlas of the human brain* Stuttgart: Thieme.

Tuch DS, Reese TG, Wiegell MR, Wedeen VJ. Diffusion MRI of complex neural architecture. Neuron. 2003; 40(5):885–895. [PubMed: 14659088]

Wiegell MR, Tuch DS, Larsson HB, Wedeen VJ. Automatic segmentation of thalamic nuclei from diffusion tensor magnetic resonance imaging. Neuroimage. 2003; 19(2 Pt 1):391–401. [PubMed: 12814588]

Winer JA. The human medial geniculate body. Hear Res. 1984; 15(3):225–247. [PubMed: 6501112]

Winer JA, Chernock ML, Larue DT, Cheung SW. Descending projections to the inferior colliculus from the posterior thalamus and the auditory cortex in rat, cat, and monkey. Hear Res. 2002; 168(1–2):181–195. [PubMed: 12117520]

Winer JA, Miller LM, Lee CC, Schreiner CE. Auditory thalamocortical transformation: structure and function. Trends Neurosci. 2005; 28(5):255–263. [PubMed: 15866200]

Winer, J. A., & Schreiner, C. E. (Eds.). (2005). *The Inferior Colliculus* New York: Springer.

Wood ML, Bronskill MJ, Mulkern RV, Santyr GE. Physical MR desktop data. Journal of Magnetic Resonance Imaging. 1994; 3(S):19–26. [PubMed: 8280987]

Yvert B, Fischer C, Guenot M, Krolak-Salmon P, Isnard J, Pernier J. Simultaneous intracerebral EEG recordings of early auditory thalamic and cortical activity in human. Eur J Neurosci. 2002; 16(6): 1146–1150. [PubMed: 12383244]
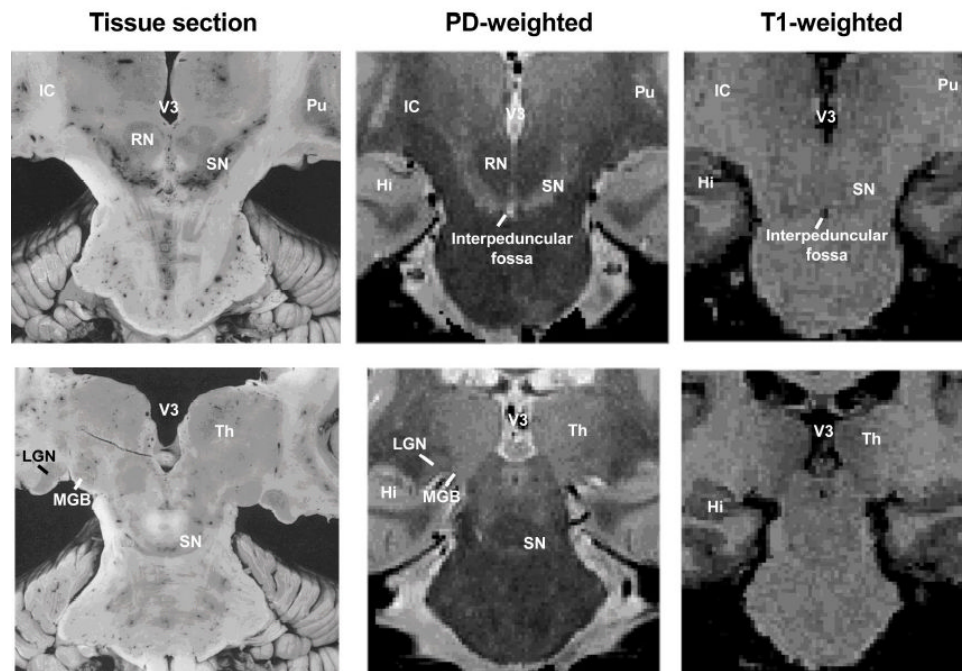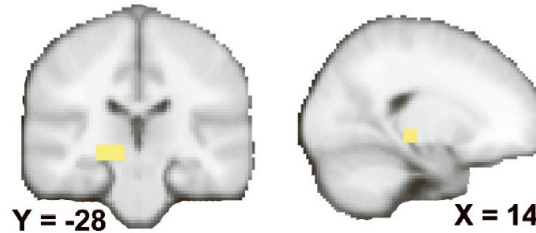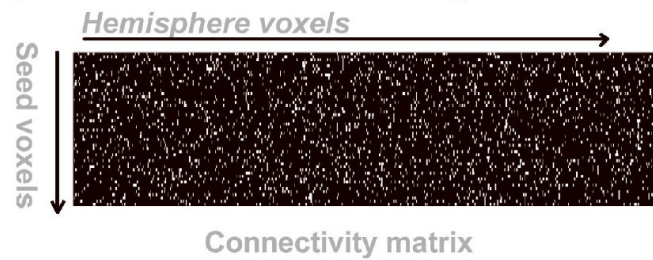
**Figure 1.**
Sections through two coronal planes used to identify MGB and LGN in the proton-density (PD) weighted images. The left panels are photographs of unstained post-mortem tissue with the temporal lobes removed. The middle and right panels are PD- and T1-weighted scans of the same sections, but from a different individual than the tissue sections. Unlike the T1 image, in the PD scan white matter appears dark (e.g. internal capsule, IC) and grey matter is lighter (e.g. substantia nigra, SN). Structures used in the visual identification of MGB and LGN are labelled where they can be seen in the images. The correspondence between the unstained tissue and PD-scan is much clearer than between the tissue and the T1 image, where reduced grey-white contrast makes it difficult to identify most of the structures. Abrevs: Hi= body of the hippocampus, IC= internal capsule, LGN= lateral geniculate nucleus, MGB= medial geniculate nucleus, Pu= putamen, RN= red nucleus, SN= substantia nigra, Th= thalamus, V3= third ventricle. The tissue photographs come from Duvernoy's (1995) Human Brain Stem and Cerebellum, pp. 292 and 301, reproduced with kind permission of Springer Science and Business Media.
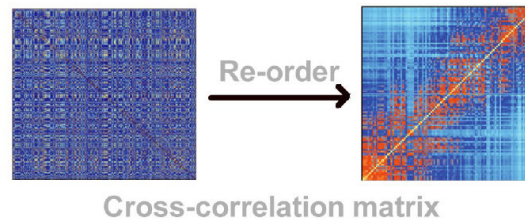
## 1. Specify the seed mask

Y = -28          X = 14

## 2. Compute tracts from each seed and generate connectivity matrix

*Hemisphere voxels*

*Seed voxels*

Connectivity matrix

## 3. Compute cross-correlation matrix and re-order

Re-order

Cross-correlation matrix

## 4. Identify clusters and map back to anatomical space

Map to T1

Clusters
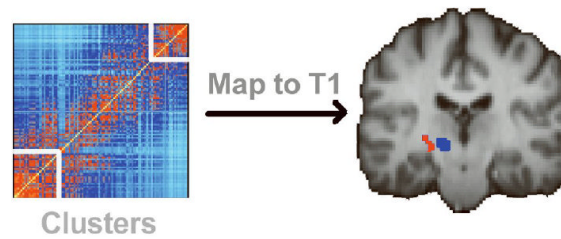
**Figure 2.**
A schematic illustration of the connectivity-based segmentation procedure. First the region-of-interest is defined in standard space then tractography is run from each voxel in this region. The connectivity is stored in a down-sampled, binary connectivity matrix, where cell [*i*, *j*] is 1 if there is a connection between the *i*th seed voxel and the *j*th voxel in the ipsilateral hemisphere. Note that ordering is arbitrary and therefore is not spatially meaningful. Next, the cross-correlation matrix is computed as a measure of voxel-wise similarity in connectivity patterns of seed voxels. This matrix is then re-ordered to bring higher values towards the diagonal, which has the effect of clustering voxels with similar connectivity. These clusters are identified and mapped back onto the T1 image. Voxels from within a given cluster identify an anatomical region where the voxels have similar connectivity patterns.
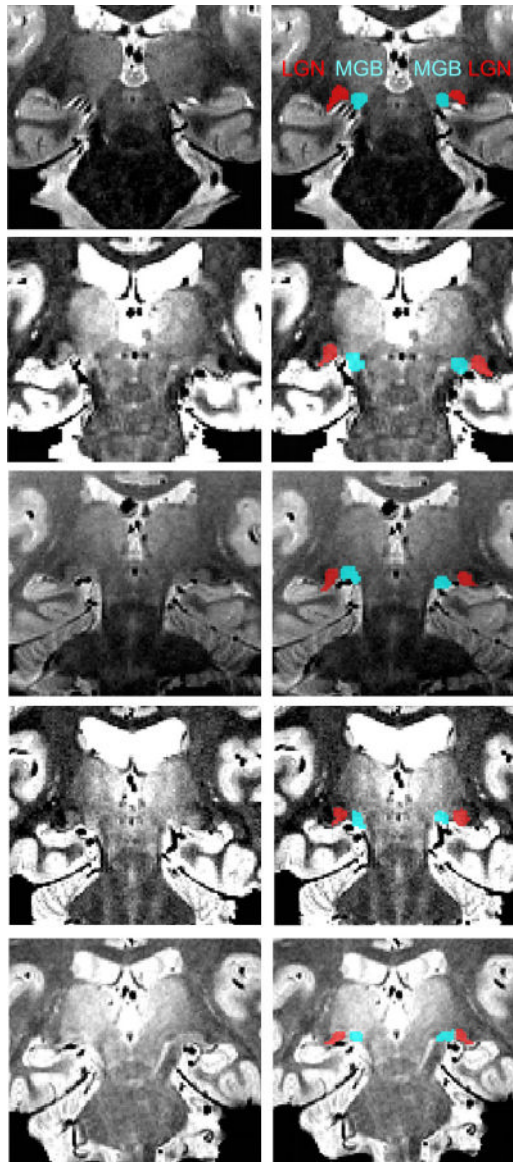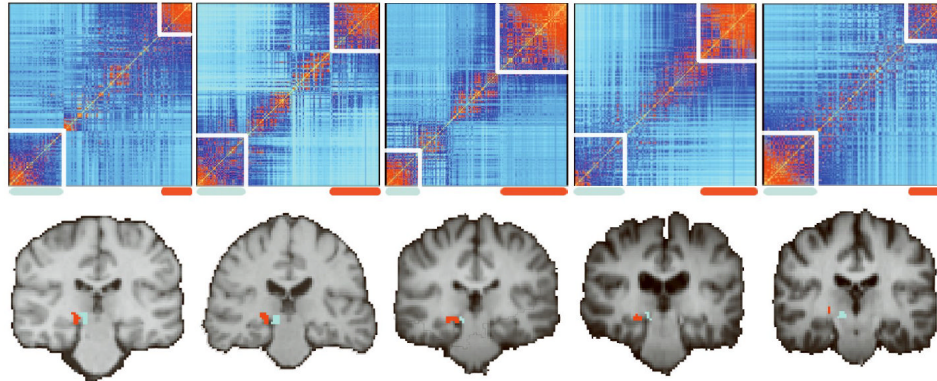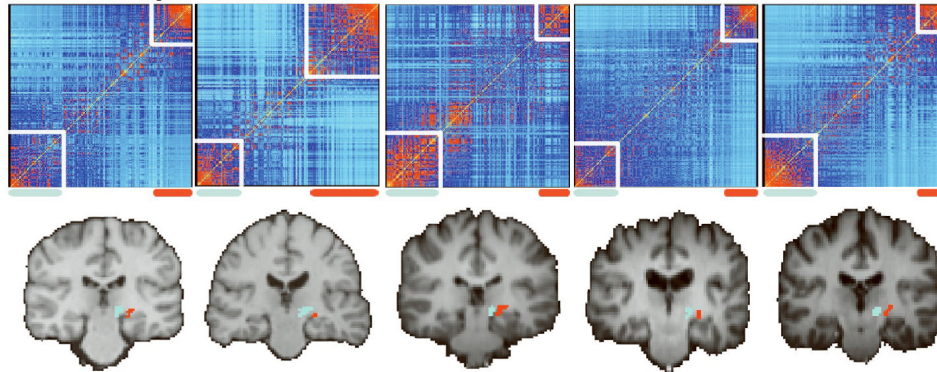
**Figure 3.**
For each participant, a coronal slice through the medial (blue) and lateral (red) geniculate bodies is shown. On the left, the PD-weighted image is presented without the masks to highlight nuclei in the raw image and on the right, the same image is shown with the nuclei in color. In both cases, the background images are displayed at a high image contrast to enhance the visibility of the nuclei. LGN typically appears as a tear-dropped shaped region of high signal intensity at the ventro-lateral edge of the thalamus. It is bordered medially by MGB which appears as an ovoid region of high intensity.

**Right hemisphere**

**Left hemisphere**

**Figure 4.**
Connectivity-based identification of the MGB (blue) and LGN (red) are shown for all five participants in both hemispheres. The top row illustrates each participant's re-ordered cross-correlation matrix with the two strongest clusters highlighted with white lines. The corresponding anatomical regions are shown below on the participant's T1 image transformed into standard space.
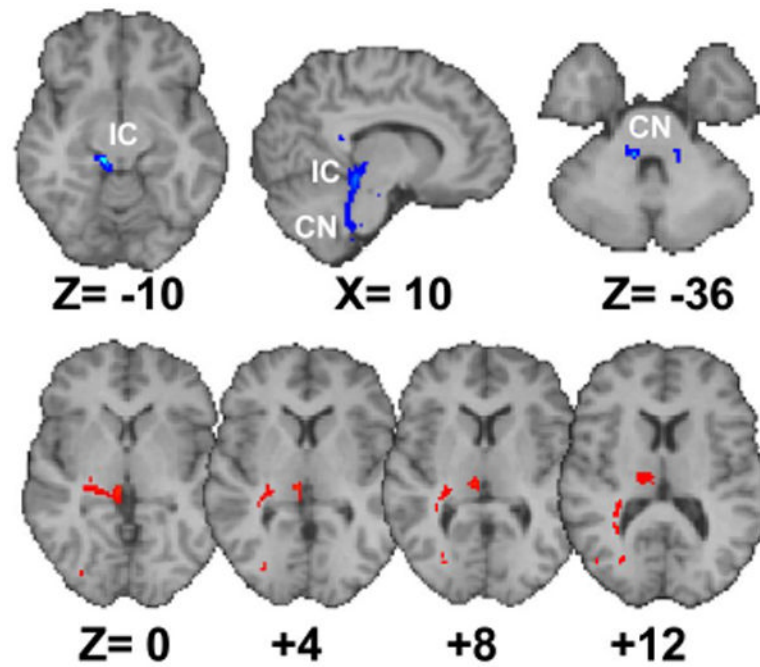
**Figure 5.**
Anatomical paths delineated by probabilistic tractography from the medial (blue) and lateral (red) cluster identified by the connectivity based segmentation algorithm. In the top row, a pathway links the medial cluster to the ipsilateral inferior colliculus and continues bilaterally to the level of the cochlear nucleus, consistent with the connectivity of the auditory pathway. In the bottom row, the path from the lateral cluster proceeds laterally and then posteriorly through Meyer's loop, connecting with occipital pole regions, consistent with thalamocortical projections between LGN and visual cortex.
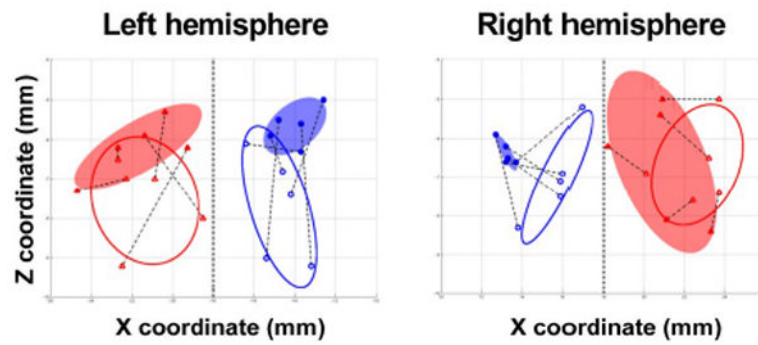
**Figure 6.**
Co-localisation of PD and DTI based segmentation of MGB and LGN. MGB centres-of-gravity are marked with small circles while the LGN is marked with triangles. Open and closed markers indicate PD- and DTI- based values, respectively. 85% confidence intervals are shown as large ovals surrounding each cluster of markers. Open ovals indicate confidence intervals for the PD-based values while filled ovals indicate confidence associated with DTI-based values.

**Table**

Standard space coordinates for the medial and lateral geniculate bodies as identified by proton density (PD) based segmentation and diffusion tensor imaging (DTI) based segmentation, per subject per hemisphere. The coordinates represent the centre of gravity for each region.

| | MGB | | | | | | LGN | | | | | |
|---|---|---|---|---|---|---|---|---|---|---|---|---|
| | Left | | | Right | | | Left | | | Right | | |
| *Subject 1* | | | | | | | | | | | | |
| PD | −13 | −29 | −9 | 14 | −28 | −8 | −19 | −29 | −8 | 20 | −28 | −7 |
| DTI | −14 | −24 | −6 | 13 | −24 | −6 | −21 | −27 | −6 | 18 | −27 | −6 |
| *Subject 2* | | | | | | | | | | | | |
| PD | −15 | −25 | −9 | 16 | −25 | −7 | −23 | −25 | −9 | 23 | −24 | −7 |
| DTI | −15 | −25 | −6 | 13 | −24 | −6 | −20 | −28 | −6 | 21 | −27 | −5 |
| *Subject 3* | | | | | | | | | | | | |
| PD | −14 | −29 | −7 | 16 | −29 | −7 | −21 | −29 | −7 | 22 | −29 | −8 |
| DTI | −13 | −26 | −5 | 13 | −25 | −7 | −20 | −28 | −5 | 21 | −26 | −8 |
| *Subject 4* | | | | | | | | | | | | |
| PD | −15 | −26 | −7 | 16 | −27 | −8 | −22 | −26 | −7 | 24 | −25 | −7 |
| DTI | −15 | −26 | −6 | 13 | −27 | −7 | −25 | −26 | −7 | 23 | −26 | −7 |
| *Subject 5* | | | | | | | | | | | | |
| PD | −16 | −29 | −6 | 16 | −28 | −5 | −23 | −27 | −7 | 24 | −28 | −5 |
| DTI | −14 | −24 | −6 | 14 | −24 | −7 | −23 | −26 | −6 | 21 | −24 | −7 |